Vibrational Fingerprints of Low-Lying Pt_nP_{2n} (n=1-5) Cluster Structures from Global Optimization based on DFT Potential Energy Surfaces.

Journal:	*The Journal of Physical Chemistry*
Manuscript ID	jp-2015-08495y.R1
Manuscript Type:	Special Issue Article
Date Submitted by the Author:	13-Nov-2015
Complete List of Authors:	Jedidi, Abdesslem; KAUST, Catalysis Center Li, Rui; UPPA IPREM ECP Fornasiero, Paolo; University of Trieste, Department of Chemical and Pharmaceutical Sciences and ICCOM Trieste Research Unit ; University of Trieste, Department of Chemical and Pharmaceutical Sciences Cavallo, Luigi; King Abdullah University of Science and Technology, Chemical and Life Sciences and Engineering, KAUST Catalysis Center Carbonniere, Philippe; UPPA IPREM ECP

Vibrational Fingerprints of Low-Lying Pt_nP_{2n} (n=1-5) Cluster Structures from Global Optimization based on DFT Potential Energy Surfaces.

Abdesslem Jedidi,[1] Rui Li,[2] Paolo Fornasiero,[3] Luigi Cavallo,[1] Philippe Carbonniere[2]

[1] Division of Physical Sciences and Engineering, KAUST Catalysis Center, King Abdullah University of Science and Technology (KAUST), 4700 KAUST, Thuwal 23955-6900, Saudi Arabia

[2] Groupe de Chimie Théorique et Réactivité, IPREM/ECP UMR CNRS 5254, Université de Pau et des Pays de l'Adour, F-64000 Pau, France

[3] Department of Chemical and Pharmaceutical Sciences, INSTM, ICCOM-CNR, University of Trieste, Via L. Giorgieri 1, 34127 Trieste, Italy

Abstract

Vibrational fingerprints of small Pt_nP_{2n} (n=1-5) clusters were computed from their low-lying structures located from a global exploration of their DFT potential energy surfaces with the GSAM code. Five DFT methods were assessed from the CCSD(T) wavenumbers of PtP_2 species and CCSD relative energies of Pt_2P_4 structures. The eight first Pt_nP_{2n} isomers found are reported. The vibrational computations reveal (i) the absence of clear signatures made by overtone or combination bands due to very weak mechanical and electrical anharmonicities (ii) some significant and recurrent vibrational fingerprints in correlation with the different PP bonding situations in the Pt_nP_{2n} structures.

Keywords

Platinum phosphide, global optimization, clusters structure, natural bond orbital analysis, vibration frequency, DFT.

1. Introduction

Due to their peculiar and tunable physico-chemical properties, materials at the (sub)nanometer level are playing an increasing role in all the area of science and technology and namely in catalysis, in which (sub)nanoclusters can exhibit strong enhanced catalytic activity compared to their corresponding bulk material[1,2]. To deeply understand the origin of this peculiar behavior work is focused on characterizing thoroughly these materials, with one of the most difficult tasks simply consisting in determining their chemical structure at the atomic level.

Experimental information on neutral or charged cluster structures can be gained, in the absence of perturbing interactions with environment or support, from gas phase infrared spectroscopy[3,4]. The vibrational fingerprints are then compared to their theoretical counterpart for a given structure predicted by quantum chemistry. In turn, the proper computation of vibrational properties is related to the proper determination of the chemical structure. This task is particularly non trivial for atomic or molecular clusters since no simple chemical rules exist to guess their structures. Thus, for such systems, (an)harmonic vibrational computations should start from reliable experimental structures, if available, or from a global optimization method[5] able to locate the proper set of low-lying minima on the potential energy surface. This last issue is a more reliable alternative to the structure prediction obtained "by hand" which means from virtual manipulation of the atomic positions or from the corresponding bulk lattice. For these reasons, in this work we focus on the characterization of low energy structures of metal phosphides from global optimization (GO) methods based on density functional theory (DFT).

Different GO methods have been developed. The first set of methods is based on thermodynamics principles in which the temperature of the system is introduced to guide the morphological evolution of the nanocluster toward the global minimum. This is the case of

molecular dynamics (MD)[6] and Monte Carlo (MC)[7] approaches. The simulated annealing (SA)[8] approaches, combined with MC or MD, consists in cooling down the system at different steps of its morphological evolution to locate the global minimum. Because of these three approaches start from one initial structure, it is not guaranteed that the global minimum is reached. The second class of global optimization methods consists in several local optimizations of a given set of generated initial structures. Here the set has to be both sufficiently small and sufficiently diverse and large as well to render the global optimization method both effective and reliable. This class of algorithms, highly parallelizable by essence, can find the global and local minima but a particular care has to be taken in the generation of the initial set of structures. This is the principal point addressed in the GSAM algorithm used in the present study[9]. From this general scheme, numerous variants are designed. The genetic algorithm (GA)[10] in which evolutionary principles are adopted to identify the optimal cluster structure, consists in an small set of initial structures which are firstly optimized (parents) and from which an additional set of structures is generated (children) from half of the structures of two parents and, for a small part of them, with small modifications of coordinates (mutations). The entire set of structures are re-optimized and only the lowest energy structures are considered for the next iteration (generation). This process, based on this ethical assumption "good parents, good children" is ended when no structures changes are observed in the new selected set. The Basin hopping (BH) algorithm[11,12] can be used as a variant of the first or the second class of algorithm since it uses random hopping moves combined to local minimizations to jump from one minimum of the PES to another. Other methods are also implemented as variants attempting to make the global methods more efficient. Here we cite the Tabu search[13] and the particle swarm optimization[14].

Metal phosphides have gained a great scientific interest both from experimental and theoretical point of view, due to their promising potential as versatile catalysts[15,16]. Indeed,

while these catalysts are not new, some investigations showed their significant role in the hydroprocessing[17] for energy conversion and other applications such as optics[18] and energy storage[19-22].

Among metal phosphide compounds, transition metals phosphides form a large class comprising over 125 binary and over 80 ternary substances differing in metal identity and metal/phosphorus stoichiometry[23]. These compounds are used as alternative heterogeneous catalysts to metals, metal oxides and metal sulfides that have widespread applications in heterogeneous catalysis[24-27]. In fact, mixing the noble metal nanoparticles with heteroatoms such as phosphorus and boron is known to be an interesting tool for tuning their catalytic properties (activity and selectivity) since it modifies both the nature of the surface sites and the overall electronic properties[28].

The synthesis, nature and structure of several transition metals phosphides has been extensively described in a number of reviews[29,30]. For instance, their structure can exhibit a variety of stoichiometries for the same metal atom. For example, it is known that nickel phosphide can have eight different structures that are Ni_3P, Ni_5P_2, $Ni_{12}P_5$, NiP_2, Ni_5P_4, NiP, Ni_2P and NiP_3[31]. At variance with Ni, platinum phosphides are known with only two stoichiometries: PtP_2 (phosphorus rich compound) and Pt_5P_2 (metal rich compound)[32,33]. Platinum phosphides with careful control over both the composition and the morphology, can be obtained by decomposition of Platinum phosphine complexes to metal phosphide nanocluster from thermal treatment under reducing conditions at 700°C[32] or from the conversion of preformed Platinum nanoparticles into metal phosphides by solution-mediated reaction with trioctylphosphyne at 300-360°C[33]. Concerning the last method, the nanocluster can be made separately according to the literature methods. On that point template-based methods have been successfully used to synthetize Pt clusters on the sub-nanometre scale[34].

In this study, we will focus on the phosphorus rich structure, PtP_2, which is the stoichiometry used as a molecular precursor and a final nanocomposite[32]. The size evolution of the PtP_2 cluster can be correlated with the vibrational spectra in order to draw the trend made from small to larger clusters[35,36]. While several theoretical studies have focused on pure platinum clusters[37,38], research on platinum phosphide clusters is lacking, although theoretical calculation have been performed on the bulk structure of PtP_2, with determination of the lattice parameter and of the vibrational frequencies, which were compared with experimental results[39].

For this paper, we report DFT calculations for Pt_nP_{2n} (n=1-5) clusters, in order to provide the lowest energy structures and the corresponding vibrational fingerprints. Particularly, the shifts of the PP stretching will be discussed in correlation with the different bonding situations in the cluster structures. Further, CCSD and CCSD(T) levels of theory were used to validate the DFT results.

II. Computational details

The structure of Pt_nP_{2n} (n = 1-5) clusters were investigated by the GSAM algorithm[40] (Global Search Algorithm of Minima), connected with the G09-d01 version of Gaussian[41] for the computation of their energies at the DFT level of theory. The GSAM code has been applied successfully for the structural investigation of binary clusters such as gallium arsenide (Ga_nAs_m, $5 < n + m < 8$)[42], tin telluride (Sn_nTe_n, n = 2−8)[43] and aluminum-based clusters[44,45] ($Si_{n-1}Al$, n = 3−10 and Al_nL_n with L = H or Cl and n = 4−7) and for the investigation of the vibrational fingerprints of molecular clusters such as microhydrated cytosine (C,nH_2O, n = 1−5)[46] and microhydrated sodium nitrate ($(NaNO_3,nH_2O)_x$, n = 1-3, x = 1-3)[47]. Here we recall that the algorithm starts with the generation of an initial set of structures by two generation modes in the present study (i) a simple random generation in a 3D space and (ii) a spheroid

generation. Thus 100+4; 300+30; 800+220; 600+1126; 400+4364 random+spheroid initial structures were generated for n ranging from 1 to 5. It is emphasized that the method relies on the so-called "raking optimization"[9]: during m steps (here m = 4), the structures are partially optimized (here 15 cycles of optimization per step, *i.e* 60 cycles after the 4 steps) and discarded step after step when they appear too high in energy compared to the lowest energy structure at each step. This energetic criterion, initially very coarse, is progressively tightened during the process ($\Delta E_{m=1}$=6.0 eV; $\Delta E_{m=2}$=4.0 eV; $\Delta E_{m=3}$=3.0 eV; $\Delta E_{m=4}$=2.0 eV). Between each successive partial optimization, a topological criterion[48] based on a concept of similarity between structures from the Minkowski metrics, is applied to discard structures topologically similar (higher than 95% in the present work). Full optimization and frequency computations are then performed for the remaining structures after the fourth step.

Five DFT methods (B3LYP[49,50], B97-2[51], PBE0[52], TPSSh[53], PW91[54]) were used to investigate the PtP_2 and Pt_2P_4 clusters, and to select the most pertinent model chemistry for investigating the Pt_3P_6, Pt_4P_8 and Pt_5P_{10} clusters. In the absence of experimental data, energy and frequencies from the DFT calculations were compared with their CCSD(T) and CCSD counterparts. In the same way three basis sets combining relativistic pseudopotentials for Platinum and all electron basis sets for Phosphorus were used. They are mentioned hereafter as BS1 (cc-pVTZ-PP[55] for Pt and cc-pVTZ[56] for P), BS2 (Def2-SVP[57] for Pt and cc-pVTZ for P) and BS3 (Def2-SVP for Pt and aug-cc-pVTZ[56] for P). During the global optimization the systems were considered in the singlet state. However, for each cluster size, the low lying structures, between 0 and 1.5 eV, were re-optimized in the triplet and quintet spin-states. Natural Bond Orbital analysis was performed with the NBO 5.9 program[58]. Anharmonic frequency analysis was performed for the low-lying structures with the g09 package[59,60] to estimate the importance of the mechanical and electrical anharmonicities on the theoretical pictures of IR spectra.

Concerning the computer resources, the computations was supported by the PYRENE cluster at the University of Pau et des Pays de l'Adour, France (23 nodes, ten core per node, Intel®Xeon®E5-2650Lv2, 32 Go RAM, Ivy Bridge EN 64 bits) and by the High Performance Computing center of TGCC, CEA, France (Supercomputer Curie Large, 1440 nodes, eight cores per node, Intel®Nehalem-EX X7560). In reason of fair-sharing and quotas, the number of jobs running in parallel ranged between 20 and 300, which leads to a real computational time ranging between several minutes and several days for each investigation (global optimization of each species from different DFT, harmonic and anharmonic frequencies).

III. Results and Discussion

A-Calibration of the model chemistry

In the absence of experimental data, the choice of the theoretical reference is guided by the best balance between accuracy and computational cost with respect to the relative energy and wavenumbers calculated for the two PtP_2 conformers in the singlet state. The corresponding CCSD(T), CCSD and DFT results are reported in Table 1 for the three basis sets mentioned in the previous section. The results reveal that only the CCSD(T) level of theory can be taken as reference for the DFT vibrational wavenumbers, since discrepancies up to 30-40 cm^{-1} are observed between the CCSD and the CCSD(T) methods (namely for the stretching P-P of the $C_{\infty v}$ species and the symmetric stretching of the C_{2V} species). On the other hand, our results also indicate that the CCSD(T) wavenumbers are shifted by no more than 10 cm^{-1} with a change of the basis set. This retains the choice to the cheapest basis set (BS2) for the DFT computations. Although the vibrational results from DFT methods are much less sensitive with the change of the basis set than their ab initio counterpart[61,62], a series of preliminary trials made with several Pople basis sets on Phosphorus reveals that further economy on the basis set does not lead to the same accuracy. Focusing on the DFT method, it arises from

Table 1 that the TPSSh/BS2 model chemistry is a good candidate for the evaluation of the vibrational properties in the Pt_nP_{2n} series. Furthermore, the relative energy of the most stable $^3PtP_2$ and $^5PtP_2$ structure (C_{2v}) are 1.26 eV and 2.08 eV above the most stable $^1PtP_2$.

Table 1 : harmonic wavenumbers (in cm^{-1}) and relative energies (in eV) of the two lowest structures found for $^1PtP_2$ species from various model chemistry (GS=Ground State).

structure	mode	CCSD(T)			CCSD			B3LYP	B97-2	PBE0	TPSSh
		BS1[(a)]	BS2[(b)]	BS3[(c)]	BS1	BS2	BS3	BS2	BS2	BS2	BS2
 GS	$\nu_{asym\ Pt\text{-}P}$	291	293	292	301	302	299	270	287	284	287
	$\delta_{P\text{-}Pt\text{-}P}$	339	344	346	342	342	349	322	338	348	339
	$\nu_{sym\ Pt\text{-}P}$	646	646	645	684	684	682	665	690	676	665
	$\delta_{P\text{-}Pt\text{-}P}$	127	130	143	134	137	150	121	128	129	129
	$\nu_{Pt\text{-}P}$	353	358	361	354	361	364	335	347	363	348
	$\nu_{P\text{-}P}$	853	863	863	886	895	896	853	881	893	863
	$\Delta E_{rel.}$ (eV)	*0.80*	*0.75*	*0.70*	*0.79*	*0.76*	*0.71*	*0.66*	*0.71*	*0.78*	*0.80*

[(a)]BS1 : cc-pVTZ-PP for Pt and cc-pVTZ for P
[(b)]BS2 : Def2-SVP for Pt and cc-pVTZ for P
[(c)]BS3 : Def2-SVP for Pt and aug-cc-pVTZ for P

The TPSSh/BS2 model chemistry was used for the global optimization of the Pt_2P_4 species.

The 26 structures of $^1Pt_2P_4$ found below 2.0 eV from the ground state at the TPSSh/BS2 level of theory were re-optimized in the triplet and quintet spin-state. The most stable $^3Pt_2P_4$ and $^5Pt_2P_4$ were found 1.05 eV and 2.45 eV above the most stable ^{1}Pt2P4 species.

Focusing on the results based on the exploration of the potential energy surface in the singlet spin-state, the structures were all of them re-optimized at the B3LYP, B97-2, PBE0 and PW91 levels of theory with the same basis set and at the CCSD level of theory with the BS3 basis set. Moreover, the validity of the CCSD/BS3 reference was assessed from single point CCSD(T)/BS3 calculations at the CCSD geometries. Table 2 reports the relative energy for the ten lowest $^1Pt_2P_4$ structures found with each computational model. Even though all the DFT methods used in the present study are able to provide the same geometry for the three

lowest structures, the TPSSh/BS2 model chemistry appears as the most robust since the ranking of the different geometries with this functional matches that provided by the CCSD method. This is in line with previous work on $Pt_nAr_m^+$ cluster structures investigated at the TPSS/def2-TZVP level of theory[63]. Moreover, we also found that some functionals, such as the B97-2 and PBE0 functionals, miss the 6th isomers by systematically leading to the 5th during the optimization.

n	Structure	CCSD	B3LYP	B97-2	PBE0	TPSSh	PW91
1		0.00	0.00	0.00	0.00	0.00	0.00
2		0.32 (7.4)	0.31 (7.1)	0.25 (5.8)	0.26 (6.0)	0.28 (6.4)	0.32 (7.4)
3		0.53 (12.2)	0.36 (8.3)	0.49 (11.3)	0.60 (13.8)	0.45 (10.4)	0.62 (14.3)
4		0.94 (21.6)	0.91 (20.9)	0.49 (11.3)	0.83 (19.1)	0.70 (16.1)	0.74 (17.0)
5		1.01 (23.2)	1.06 (24.4)	1.10 (25.3)	1.02 (23.5)	0.86 (19.8)	0.89 (20.5)
6		1.03 (23.7)	1.00 (23.0)	-	-	0.97 (22.3)	0.91 (20.9)
7		1.16 (26.7)	1.06 (24.4)	1.16 (26.7)	1.18 (27.1)	0.98 (22.5)	1.06 (24.4)
8		1.22 (28.1)	0.96 (22.1)	1.13 (26.0)	1.19 (27.4)	1.02 (23.5)	0.95 (21.8)
9		1.26 (29.0)	0.80 (18.4)	1.16 (26.7)	1.30 (29.9)	1.11 (25.5)	1.07 (24.6)
10		1.32 (30.4)	1.03 (23.7)	1.25 (28.7)	1.45 (33.4)	1.39 (31.9)	1.42 (32.7)

Table 2 : The first ten relative energies (in eV, and kcal.mol^{-1} in parenthesis) of the $^1Pt_2P_4$ structures computed with different DFT methods with the BS2 basis set and compared with the CCSD/BS3 level of theory. (The grey shaded zones correspond to structures incorrectly graded for the DFT used with respect to the CCSD results).

B- Structures and bonding

In Figure 1 are reported the eight most stable structures of each $^1Pt_nP_{2n}$ species (n=2-5) in terms of relative Gibbs energy found from GSAM at the TPSSh/BS2 level of theory. As by-product, the evolution of the binding energy in the series is provided in the supplementary material. We mention that the first triplet spin-state structures are found at 1.05, 0.45, 0.85 and 1.20 eV above the most stable $^1Pt_nP_{2n}$ structure for n going from 2 to 5, respectively. Moreover, and considering the temperature of their synthesis, a Boltzmann probability of 5% corresponds to a relative energy of 0.2-0.25 eV.

Most of the clusters have no symmetry (C_1) or exhibit a low symmetry with a mirror plane only (C_S). Some species with higher symmetry group are found (D_{2d} for Pt_2P_4 at 0.28 eV and C_2 for Pt_3P_6 at 0.31 eV), but they do not correspond to a global minimum, disqualifying investigations made "by hand" or from bulk lattice. The structural investigation is rendered even more difficult because of the absence of clear building block for these species: two sub-units of PtP_2 as building blocks do not lead to one Pt_2P_4 (2a) ; the Pt_3P_6 (3a) cluster is made from one PtP_2 (1a) and one Pt_2P_4 (2a) sub-units, while Pt_3P_6 (2b) is built from three PtP_2 (2a) sub-units as building blocks ; Pt_4P_8 and Pt_5P_{10} structures cannot be deduced from smaller size species. This observation also discredits the efficiency of a simpler and by far faster global optimization scheme which would consider these atomic clusters as random combinations of molecular sub-units. For instance, our global search process miss the 2a and 3a structures and find 5c as the lowest energy Pt_5P_{10} structure when considering the Pt_nP_{2n} clusters as n(PtP_2) species.

Figure 1: Relative Gibbs energies (ΔG in eV) for the most stable $^{1}Pt_nP_{2n}$ clusters (n=2-5) found from the global exploration of their TPSSh/BS2 PES.

	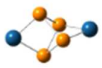						
2a (Cs)	2b (D2d)	2c (Cs)	2d (Cs)	2e (C1)	2f (C1)	2g (C1)	2h (C1)
ΔG=0.00 eV	ΔG=0.28 eV	ΔG=0.37 eV	ΔG=0.65 eV	ΔG=0.84 eV	ΔG=0,92 eV	ΔG=0,93 eV	ΔG=0,96 eV
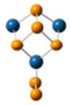				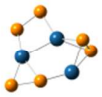	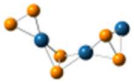		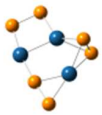
3a (Cs)	3b (Cs)	3c (C1)	3d (C1)	3e (C1)	3f (C1)	3g (C2)	3h (Cs)
ΔG =0.00 eV	ΔG =0.02 eV	ΔG =0.25 eV	ΔG =0.27 eV	ΔG =0.27 eV	ΔG =0.29 eV	ΔG =0.31 eV	ΔG =0.33 eV
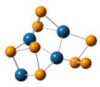	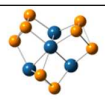	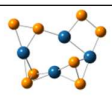			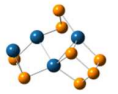		
4a (C1)	4b (C1)	4c (C1)	4d (C1)	4e (C1)	4f (C1)	4g (C1)	4h (C1)
ΔG =0.00 eV	ΔG =0.22 eV	ΔG =0.18 eV	ΔG =0.23 eV	ΔG =0.42 eV	ΔG =0.37 eV	ΔG =0.51 eV	ΔG =0.54 eV
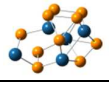			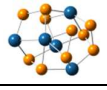		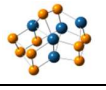		
5a (C1)	5b (C1)	5c (Cs)	5d (C1)	5e (C1)	5f (C1)	5g (Cs)	5h (C1)
ΔG =0.00 eV	ΔG =0.13 eV	ΔG =0.15 eV	ΔG =0.25 eV	ΔG =0.26 eV	ΔG =0.26 eV	ΔG =0.45 eV	ΔG =0.50 eV

The P-P bond lengths range from 2.0 Å to 2.3 Å in the series. The computation of P-P bonds lengths for P≡P, HP=PH and H2P-PH2 molecules at the TPSSh/BS2 level of theory yield 1.90 Å (expt=1.89 Å), 2.03 Å and 2.25 Å, respectively. Alternations of P2 motifs separated by Pt atoms (PP distance < 2.15 Å) lead to quasi-planar structures while the presence of P3 or P4 motifs (PP distance > 2.15 Å) confer to the cluster a more compact structure. The different bonding situations from Natural Bond Orbital (NBO) analysis are listed below. Moreover the donor-acceptor interactions provided here-after emerge from the second order perturbation theory analysis of Fock Matrix in NBO basis.

(i) A triple bounded P≡P unit interacting with Pt atom in bridge site (2c, 3a). The NBO analysis indicates also a very strong π donation from π PP to the metal center ($\Delta E^{(2)}$>400 kcal.mol^{-1}). This bonding situation can be described rather as a P=P double bond (1.99 Å in

2c, 1.98 Å in 3a) with two σP-Pt bonds (2.36±0.04 Å in 2c, 2.40±0.05 Å in 3a). This is confirmed by the Wiberg bond index that shows a bond order of 2.3 for the PP bond and 0.5 for each of the two PtP bonds (3a).

(ii) A triple bounded P≡P unit bounded to one Pt atom in bridge site, plus one of the two P atoms bounded collinearly to a second Pt atom in the P-P-Pt plane (3b, 4c). Concerning the P2 unit, the NBO analysis indicates the same bonding situation than those previously described and yields for the present case a P=P double bond (2.00 Å in 3b and 1.99 Å in 4c) and two σP-Pt bonds (2.35±0.02 Å in 3b, 2.35±0.05 Å in 4c) . Moreover, a strong stabilizing interaction of the P lone pair in the Pt center was found (nPP→Pt, ($\Delta E^{(2)}$ =100 kcal.mol^{-1}) corresponding to a σP-Pt bond (2.26 Å in 3b, 2.19 Å in 4c). The corresponding Wiberg bond indexes are 1.98, 0.55, 0.55 and 0.54, respectively (3b).

(iii) A triple P≡P unit bridged in a syn-periplanar manner to a Pt2 unit (3e, 4c) in which one of the π orbital of the PP triple bond interacts with each of the two virtual dz2 orbitals of the Pt2 unit. The bond length of the P2 unit is calculated at 2.02 Å in 4c.

(iv) A triple bounded P≡P unit bridged perpendicularly to a Pt2 unit (2c, 3b, 4a, 4c). Here each of the two occupied π orbitals of the P2 unit interacts with each of the two virtual dz2 orbitals of the Pt2 unit. This could be visualized as one PP single bond (2.06 Å in 4c, bond index=1.7) and four σP-Pt bonds (2.42±0.06 Å in 4c, bond index=0.5).

(v) A P2 unit bridged to a triangular Pt3 unit (3c, 4b, 5b). 2nd order perturbation theory analysis renders difficult to draw a simple picture here. However, the Wiberg bond index is 1.5 for the PP bond, 0.45±0.05 for each of the Pt-P bonds and almost 0 for the Pt-Pt bonds. The PP bond appears as an intermediate between single and double bond, in agreement with a bond distance around 2.12 Å for the three species.

(vi) P3 units (triangle) and P4 units (trigonal pyramid) are all of them sigma bounded (PP distance = 2.25±0.05 Å, bond index = 1.0). These units are bounded to Pt2 or Pt3 units (PtP

distance = 2.30±0.05 Å for which the bond index range from 0.5 to 1.0). Considering the most stable species of Pt_4P_8 and Pt_5P_{10}, the structural evolution seems to tend toward a network of PP single bonds.

To conclude, the NBO analysis shows that the PP bond length (from 2.0 to 2.3 Å) increases with the weakness of the PP double bond (bond index from 2.3 to 1.0). This can be correlated with the position of the PP stretching in the IR spectra of the Pt_nP_{2n} series, as described below.

C- Vibrational fingerprints

The anharmonic vibrational spectra of the structures lying below 0.25 eV are reported in Figure 2. The spectra are shaped from convolution of the computed transition with pure Lorentzian profiles of 10 wavenumber width. As expected for these systems, the mechanical anharmonicity is weak: the anharmonic shifts are more related to the quasi-degeneracy between some vibrational levels than the strength of their coupling. In any case, the maximum anharmonic shift is lower than 10 wavenumbers in the series. Electrical anharmonicity is also weak, which does not change the picture provided by the harmonic description of IR spectra: here, the highest anharmonic intensities of overtones and combination bands are lower than 0.1 $km.mol^{-1}$.

Overall, the vibrational pictures are marked by the fingerprint of the PP motif in the Pt_nP_{2n} series (n=2-5) for which the redshift increases with the decreasing bond order. Starting from the highest wavenumbers, the first transition appears at around 700 cm^{-1} (see spectra of 3a, 3b, 4c and 4d species) and corresponds to a stretching motion of a P2 unit bounded to one Pt atom in bridge site only (case i) or with a further Pt atom collinear to the PP bond (case ii). Next, a transition at around 600 cm^{-1} (see spectra of 3b, 4a, 4c and 4d species) reveals the presence of a P2 unit bounded to a Pt2 unit in a eclipsed or staggered position (case iii and iv, respectively). The signal in the range 580-500 cm^{-1} corresponds to two kinds of fragments

(case v and vi): either the stretching of a P2 unit bounded to a Pt3 unit (515 cm^{-1} for 4b, 546 cm^{-1} and 500 cm-1 for 5b), either the breathing motion of a P3 unit bounded to a Pt2 unit (573 cm^{-1} for 3c). The breathing motion of a P3 unit bounded to a Pt3 unit appears slightly redshifted at 500-480 cm^{-1} (502 and 479 cm^{-1} for 4b, 478 cm^{-1} for 5b). One of the most intense and significant fingerprints is situated at around 400 cm^{-1} which corresponds to the stretching region of single bounded Phosphorus atoms (case vi). While the structural evolution in the Pt_nP2_n series seems to tend toward a network of PP single bonds, this signal can appear redshifted or blueshifted by about 40 cm^{-1}. Thus in the series one can observe some transitions around 600-700 cm^{-1} for the quasi-planar structures or around 400-500 cm^{-1} for the compact structures. Note also a recurrent fingerprint situated at 300±50 cm^{-1} which corresponds mainly to the region of the Pt-P stretchings and does not reveals a particular layout.

Figure 2: Anharmonic vibrational spectra (position in cm^{-1}, intensity in $km.mol^{-1}$) for the most stable $^1Pt_nP_{2n}$ species (relative energy below 0.25 eV): VPT2 treatment from a TPSSh/BS2 quartic force field around each local minimum.

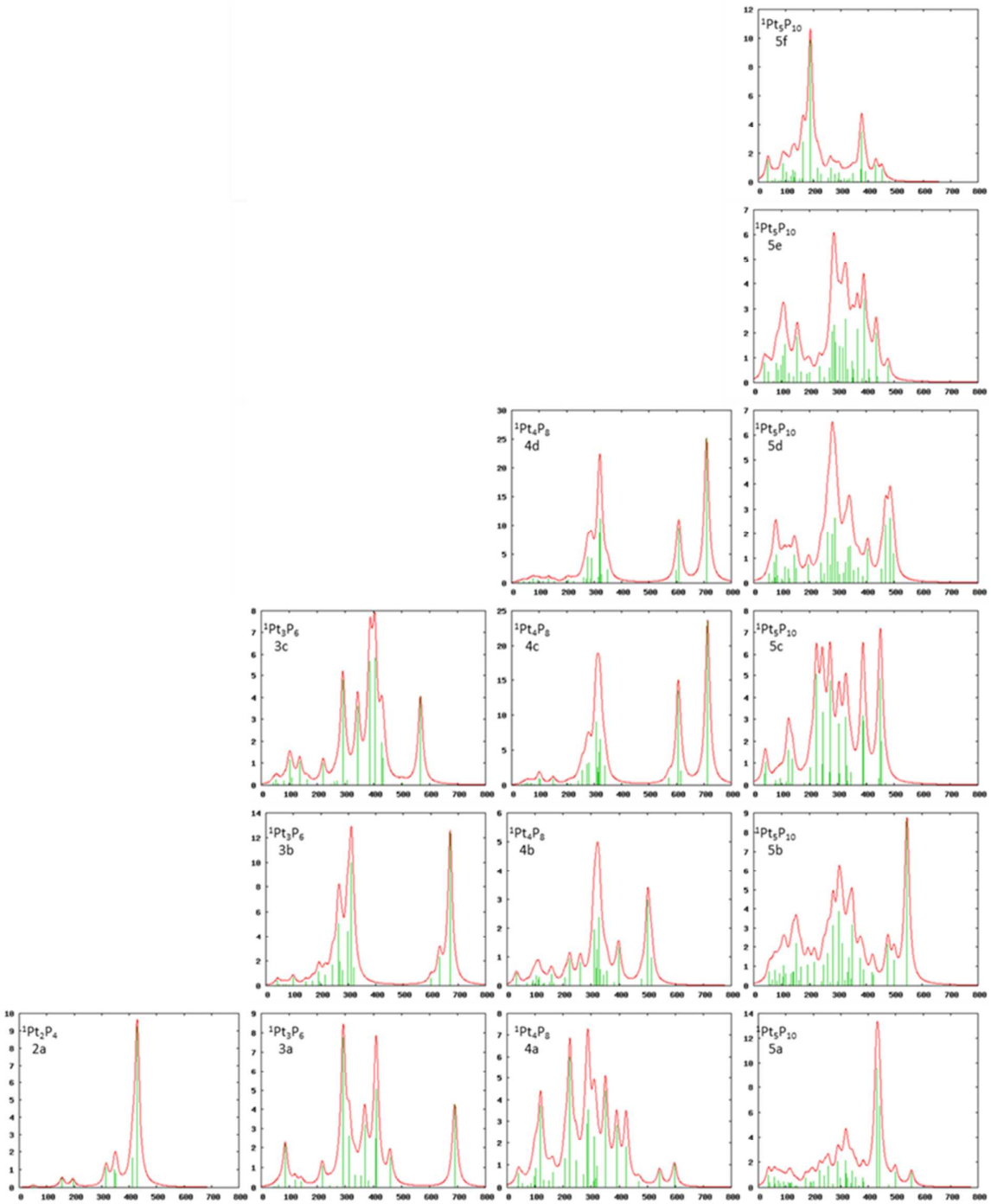

IV. Conclusion

Vibrational fingerprints of small Pt_nP_{2n} (n=1-5) clusters were computed from their low-lying structures located from a global exploration of their DFT (TPSSh) potential energy surface with the GSAM code. In absence of experimental data, the ability of the TPSSh model to produce reliable results was assessed from the CCSD(T) wavenumbers of PtP_2 species and CCSD relative energies of Pt_2P_4 structures. The global optimization reveals that most of the structures have no symmetry and no clear building blocks. The vibrational computations reveal the absence of clear signatures made by overtone or combination bands due to very weak mechanical and electrical anharmonicities. This indicates that the harmonic picture is enough to distinguish the structures. On that point, we mention at least three significant fingerprints: (i) a signal around 400 cm^{-1} reveals a rather compact structure made by triangular or "pseudo-tetrahedral" phosphorus units between two Pt atoms (ii) One or two distinct transitions between 600 and 700 cm^{-1} indicating a quasi-planar structure (iii) a signature in the range 580-480 cm^{-1} characterizing a P3 motif bonded to a Pt2 or Pt3 unit or a P2 motif bounded to a Pt3 unit.

Acknowledgment

The High Performance Computing center TGCC, CEA (Très Grand Centre de Calcul, Commissariat à l'Energie Atomique), the University of Pau and Pays de l'Adour are warmly acknowledged for their computational support. KAUST (King Abdullah University of Science and Technology) and the COST action MOLIM CM1405 are acknowledged for the financial support of the research reported in this work. The authors are grateful to Dr. Karine Miqueu for its help concerning the NBO analysis.

References

1. Haruta, M., Size- and Support-Dependency in the Catalysis of Gold. *Catal. Today* **1997,** *36* (1), 153-166.
2. Jedidi, A.; Markovits, A.; Minot, C.; Abderrabba, M., Core Restructuring for Magnetic Fe55 Icosahedral Nanoparticles. *Chem. Phys. Lett.* **2012,** *541*, 101-104.
3. Kerpal, C.; Harding, D. J.; Hermes, A. C.; Meijer, G.; Mackenzie, S. R.; Fielicke, A., Structures of Platinum Oxide Clusters in the Gas Phase. *J. Phys. Chem. A* **2013,** *117* (6), 1233-1239.
4. Asmis, K. R., Structure Characterization of Metal Oxide Clusters by Vibrational Spectroscopy: Possibilities and Prospects. *Phys. Chem. Chem. Phys.* **2012,** *14* (26), 9270-9281.
5. Heiles, S.; Johnston, R. L., Global Optimization of Clusters using Electronic Structure Methods. *Int. J. Quantum Chem* **2013,** *113* (18), 2091-2109.
6. Iwamatsu, M., Global Geometry Optimization of Silicon Clusters using the Space-fixed Genetic Algorithm. *J. Chem. Phys* **2000,** *112* (24), 10976-10983.
7. Pedroza, L. S.; Silva, A. J. R. d., Ab initio Monte Carlo Simulations Applied to a Si_5 Cluster. *Phys. Rev. B* **2007,** *75* (24), 245331.
8. Kirkpatrick, S.; Gelatt, C. D.; Vecchi, M. P., Optimization by Simulated Annealing. *Science* **1983,** *220* (4598), 671-680.
9. Marchal, R.; Carbonnière, P.; Pouchan, C., A Global Search Algorithm of Minima Exploration for the Investigation of Low Lying Isomers of Clusters from Density Functional Theory-based Potential Energy Surfaces: The example of Si_n(n=3,15) as a Test Case. *J. Chem. Phys* **2009,** *131* (11), 114105
10. Johnston, R. L., Evolving Better Nanoparticles: Genetic Algorithms for Optimising Cluster Geometries. *Dalton Transactions* **2003,** (22), 4193-4207.
11. Issaoui, N.; Abdessalem, K.; Ghalla, H.; Yaghmour, S. J.; Calvo, F.; Oujia, B., Theoretical Investigation of the Relative Stability of Na+Hen (n = 2–24) clusters: Many-body Versus Delocalization Effects. *J. Chem. Phys* **2014,** *141* (17), 174316.
12. Wales, D. J.; Doye, J. P. K., Global Optimization by Basin-Hopping and Lowest Energy Structures of Lennard-Jones Clusters Containing up to 110 Atoms. *J. Phys. Chem. A* **1997,** *101* (28), 5111-5116.
13. Glover, F., Tabu Search—Part II. *ORSA Journal on Computing* **1990,** *2* (1), 4-32.
14. Kennedy, J.; Eberhart, R. In *Particle swarm optimization*, Neural Networks, Proceedings, IEEE International Conference on, 1995; pp 1942-1948.
15. Huang, R.; Li, H.; Lin, Z.; Yang, S., Experimental and Theoretical Studies of Small Homoatomic Phosphorus Clusters. *J. Phys. Chem.* **1995,** *99* (5), 1418-1423.
16. Jones, R. O.; Ganteför, G.; Hunsicker, S.; Pieperhoff, P., Structure and Spectroscopy of Phosphorus Cluster Anions: Theory (Simulated Annealing) and Experiment (Photoelectron Detachment). *J. Chem. Phys* **1995,** *103* (22), 9549-9562.
17. Alexander, A.-M.; Hargreaves, J. S. J., Alternative Catalytic Materials: Carbides, Nitrides, Phosphides and Amorphous Boron Alloys. *Chem. Soc. Rev.* **2010,** *39* (11), 4388-4401.
18. Xie, R.; Battaglia, D.; Peng, X., Colloidal InP Nanocrystals as Efficient Emitters Covering Blue to Near-Infrared. *J. Am. Chem. Soc.* **2007,** *129* (50), 15432-15433.
19. Cabana, J.; Monconduit, L.; Larcher, D.; Palacín, M. R., Beyond Intercalation-Based Li-Ion Batteries: The State of the Art and Challenges of Electrode Materials Reacting Through Conversion Reactions. *Adv. Mat.* **2010,** *22* (35), E170-E192.
20. Carenco, S.; Surcin, C.; Morcrette, M.; Larcher, D.; Mézailles, N.; Boissière, C.; Sanchez, C., Improving the Li-Electrochemical Properties of Monodisperse Ni2P Nanoparticles by Self-Generated Carbon Coating. *Chem. Mat.* **2012,** *24* (4), 688-697.

21. Gillot, F.; Boyanov, S.; Dupont, L.; Doublet, M. L.; Morcrette, M.; Monconduit, L.; Tarascon, J. M., Electrochemical Reactivity and Design of NiP2 Negative Electrodes for Secondary Li-Ion Batteries. *Chem. Mat.* **2005,** *17* (25), 6327-6337.
22. Souza, D. C. S.; Pralong, V.; Jacobson, A. J.; Nazar, L. F., A Reversible Solid-State Crystalline Transformation in a Metal Phosphide Induced by Redox Chemistry. *Science* **2002,** *296* (5575), 2012-2015.
23. von Schnering, H. G.; Honle, W., *Encyclopedia of Inorganic Chemistry*. John Wiley & Sons: Chichester, U.K, 1994; Vol. 6.
24. Oyama, S. T., Novel catalysts for Advanced Hydroprocessing: Transition Metal Phosphides. *J. Catal.* **2003,** *216* (1-2), 343-352.
25. Oyama, S. T.; Gott, T.; Zhao, H.; Lee, Y.-K., Transition Metal Phosphide Hydroprocessing Catalysts: A review. *Catal. Today* **2009,** *143* (1-2), 94-107.
26. Chianelli, R. R.; Berhault, G.; Torres, B., Unsupported Transition Metal Sulfide Catalysts: 100 years of Science and Application. *Catal. Today* **2009,** *147* (3-4), 275-286.
27. Prins, R.; De Beer, V. H. J.; Somorjai, G. A., Structure and Function of the Catalyst and the Promoter in Co-Mo Hydrodesulfurization Catalysts. *Catal. Rev.* **1989,** *31* (1-2), 1-41.
28. Chen, Y., Chemical Preparation and Characterization of Metal-metalloid Ultrafine Amorphous Alloy Particles. *Catal. Today* **1998,** *44* (1-4), 3-16.
29. Aronsson, B.; Lundström, T.; Rundqvist, S., *Borides, Silicides and Phosphides Methuen*. London, 1965.
30. Corbridge, D. E. C., *Studies in Inorganic Chemistry*. fourth ed ed.; Elsevier: Amsterdam 1990; Vol. 10.
31. Greenwood, N. N.; Earnshaw, A., *Chem. Elements*. 1st ed.; Pergamon Press Plc: 1984.
32. Lukehart, C. M.; Milne, S. B.; Stock, S. R., Formation of Crystalline Nanoclusters of Fe_2P, RuP, Co_2P, Rh_2P, Ni_2P, Pd_5P_2, or PtP_2 in a Silica Xerogel Matrix from Single-Source Molecular Precursors. *Chem. Mat.* **1998,** *10* (3), 903-908.
33. Henkes, A. E.; Vasquez, Y.; Schaak, R. E., Converting Metals into Phosphides: A General Strategy for the Synthesis of Metal Phosphide Nanocrystals. *J. Am. Chem. Soc.* **2007,** *129* (7), 1896-1897.
34. Lu, Y.; Chen, W., Sub-nanometre Sized Metal Clusters: From Synthetic Challenges to the Unique Property Discoveries. *Chem. Soc. Rev.* **2012**, 41, 3594–3623.
35. Ingale, A.; Rustagi, K. C., Raman Spectra of Semiconductor Nanoparticles: Disorder-activated Phonons. *Phys. Rev. B* **1998,** *58* (11), 7197-7204.
36. Wang, R.-p.; Zhou, G.-w.; Liu, Y.-l.; Pan, S.-h.; Zhang, H.-z.; Yu, D.-p.; Zhang, Z., Raman Spectral Study of Silicon Nanowires: High-order Scattering and Phonon Confinement effects. *Phys. Rev. B* **2000,** *61* (24), 16827-16832.
37. Chen, Y.; Vlachos, D. G., Hydrogenation of Ethylene and Dehydrogenation and Hydrogenolysis of Ethane on Pt(111) and Pt(211): A Density Functional Theory Study. *The J. Phys. Chem. C* **2010,** *114* (11), 4973-4982.
38. García-Diéguez, M.; Finocchio, E.; Larrubia, M. Á.; Alemany, L. J.; Busca, G., Characterization of Alumina-Supported Pt, Ni and PtNi Alloy Catalysts for the Dry Reforming of Methane. *J. Catal.* **2010,** *274* (1), 11-20.
39. Meier, M.; Weihrich, R., Ab Initio Simulation of the Fundamental Vibrational Frequencies of Selected Pyrite-type Pnictides. *Chem. Phys. Lett.* **2008,** *461* (1–3), 38-41.
40. GSAM. Marchal, R.; Carbonniere, P; Pouchan, C., (Theoretical Chemistry Group, Institute of Analytical Science and Physical Chemistry for the Environment and Materials, University of Pau and the Adour region, Pau, France).
41. Frisch, M. J.; Trucks, G. W.; Schlegel, H. B.; Scuseria, G. E.; Robb, M. A.; Cheeseman, J. R.; Scalmani, G.; Barone, V.; Mennucci, B.; Petersson, G. A.; et al.; *Gaussian 09*, Gaussian, Inc.: Wallingford, CT, USA, 2009.

42. Marchal, R.; Carbonnière, P.; Begue, D.; Pouchan, C. Structural and Vibrational Determination of Small Gallium-Arsenide Clusters from CCSD(T) and DFT Calculations. *Chem. Phys. Lett*. **2008**, 453, 49-54.
43. Marchal, R.; Carbonnière, P.; Pouchan, C. Structural and Vibrational Properties Prediction of Sn_nTe_n Clusters (n = 2-8) using the GSAM Approach. *Comput. Theor. Chem*. **2012**, 990, 100-105.
44. Karamanis, P.; Marchal, R.; Carbonniére, P.; Pouchan, C. Doping Effects on the Electric Response Properties of Silicon Clusters: A Global Structure-Property Investigation of $AlSi_{n-1}$ Clusters (n = 3-10). *Chem. Phys. Lett.* **2010**, 500, 59-64.
45. Marchal, R.; Manca, G.; Kahlal, S.; Carbonnière, P.; Pouchan, C.; Halet, J.-F.; Saillard, J.-Y. Structures and Stabilities of Small, Ligated AlnLn0/2− and AlnLn+2 Clusters (L =H, Cl) − A Theoretical Study. *Eur. J. Inorg. Chem.* **2012**, 2012 (30), 4856-4866.
46. Carbonniere, P.; Thicoipe, S.; Very, T.; Assfeld, X. Vibrational Analysis beyond the Harmonicity from Ab Initio Molecular Dynamics: Case of Cytosine in Its Anhydrous and Aqueous Forms. *Int. J. Quantum Chem*. **2012**, 112, 2221-2230.
47. Carbonniere, P.; Thicoipe, S.; Pouchan, C. Theoretical Strategy to Build Structural Models of Microhydrated Inorganic Systems for the Knowledge of Their Vibrational Properties: The Case of the Hydrated Nitrate Aerosols. *J. Phys. Chem. A* **2013**, 117, 3826-3834.
48. Karamanis, P.; Carbonnière, P.; Pouchan, C., Structures and Composition-dependent Polarizabilities of Open- and Closed-shell Ga_nAs_m Semiconductor Clusters. *Phys. Rev. A* **2009,** *80* (5), 053201.
49. Becke, A. D., Density-functional Thermochemistry. III. The Role of Exact Exchange. *J. Chem. Phys* **1993,** *98* (7), 5648-5652.
50. Lee, C.; Yang, W.; Parr, R. G., Development of the Colle-Salvetti Correlation-energy Formula into a Functional of the Electron Density. *Phys. Rev. B* **1988,** *37* (2), 785-789.
51. Wilson, P. J.; Bradley, T. J.; Tozer, D. J., Hybrid Exchange-correlation Functional Determined from Thermochemical Data and Ab Initio Potentials. *J. Chem. Phys* **2001,** *115* (20), 9233-9242.
52. Adamo, C.; Barone, V., Toward Reliable Density Functional Methods without Adjustable Parameters: The PBE0 model. *J. Chem. Phys* **1999,** *110* (13), 6158-6170.
53. Tao, J.; Perdew, J. P.; Staroverov, V. N.; Scuseria, G. E., Climbing the Density Functional Ladder: Nonempirical Meta-Generalized Gradient Approximation Designed for Molecules and Solids. *Phys. Rev. Lett.* **2003,** *91* (14), 146401.
54. Perdew, J. P.; Burke, K.; Wang, Y., Generalized Gradient Approximation for Exchange-correlation Hole of a Many-electron System. *Phys. Rev. B* **1996,** *54* (23), 16533-16539.
55. Figgen, D.; Peterson, K. A.; Dolg, M.; Stoll, H., Energy-consistent Pseudopotentials and Correlation consistent Basis Set for 5d Element Hf-Pt. *J. Chem. Phys* **2009,** *130* (16), 164108.
56. Woon, D. E.; Dunning, T. H., Gaussian Basis Sets for use in Correlated Molecular Calculations. III. Atoms Aluminum through Argon. *J. Chem. Phys* **1993,** *98* (2), 1358-1371.
57. Weigend, F.; Ahlrichs, R., Balanced Basis Sets of Split Valence, Triple Zeta Valence and Quadruple Zeta Valence Quality for H to Rn: Design and Assessment of Accuracy. *Phys. Chem. Chem. Phys.* **2005,** *7* (18), 3297-3305.
58. NBO 5.9. Glendening, E. D.; Badenhoop, J. K.; Reed, A.E.; Carpenter, J.E.; Bohmann, J.A.; Morales, C. M.; Weinhold, F., (Theoretical Chemistry Institute, University of Wisconsin, Madison, WI, 2004); http://www.chem.wisc.edu/~nbo5.
59. Barone, V., Anharmonic Vibrational Properties by a Fully Automated Second-order Perturbative Approach. *J. Chem. Phys* **2005,** *122* (1), 014108.

60. Barone, V.; Biczysko, M.; Bloino, J., Fully Anharmonic IR and Raman Spectra of Medium-size Molecular Systems: Accuracy and Interpretation. *Phys. Chem. Chem. Phys.* **2014,** *16* (5), 1759-1787.
61. Carbonniere, P.; Lucca, T.; Pouchan, C.; Rega, N.; Barone, V., Vibrational Computations beyond the Harmonic Approximation: Performances of the B3LYP Density Functional for Semirigid Molecules. *J. Comput. Chem.* **2005,** *26* (4), 384-388.
62. Carbonniere, P.; Barone, V., Performances of Different Density Functionals in the Computation of Vibrational Spectra beyond the Harmonic Approximation. *Chem. Phys. Lett.* **2004,** *399* (1–3), 226-229.
63. Harding, D. J.; Kerpal, C.; Rayner, D. M.; Fielicke, A., Communication: The Structures of Small Cationic Gas-phase Platinum Clusters. *J. Chem. Phys* **2012,** *136* (21), 211103

Graphic Material for the Table of Contents